Development and Interpretation of improved Nitrous Acid Retrievals (DINAR)

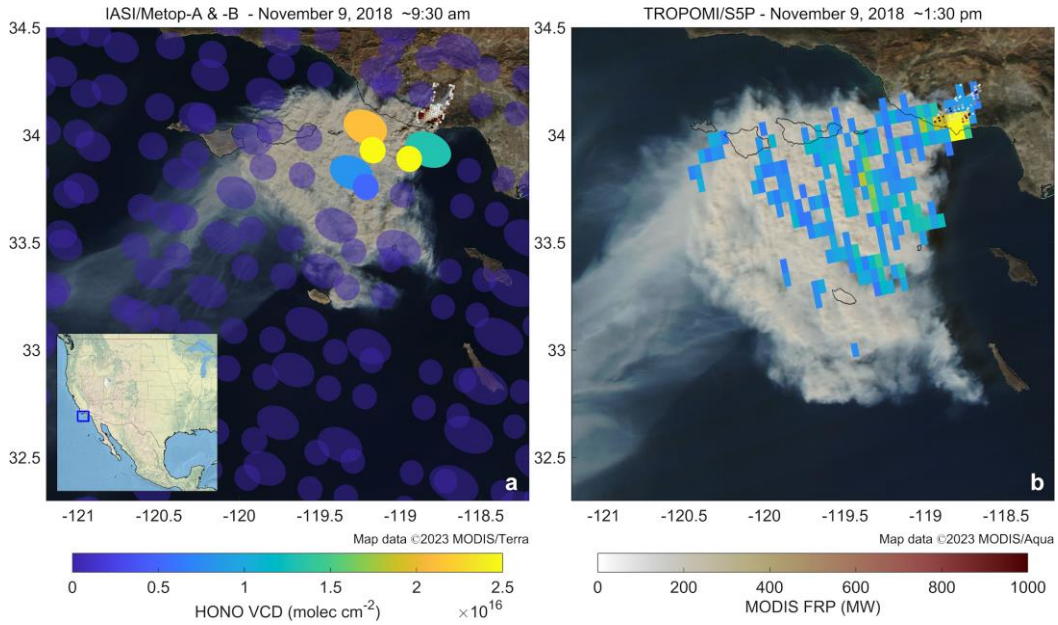

Validation Report Document

document number	:	DINAR_HONO_VR
authors	:	Bruno Franco, Nicolas Theys, Lieven Clarisse
Distributed to	:	Christian Retscher, Daniele Gasbarra
issue	:	1.2
date	:	2024-02-27
status	:	Final

Table of Contents

1 Introduction

As part of the Development and Interpretation of improved Nitrous Acid Retrievals (DINAR) project, algorithms to retrieve HONO columns from ultraviolet and thermal infrared satellite nadir observations have been developed. The retrieval algorithms were applied to measurements from the TROPOspheric Monitoring Instrument (TROPOMI) and the Infrared Atmospheric Sounding Interferometer (IASI), respectively. A description of these retrieval schemes is given in the DINAR ATBD.

The purpose of this document is to describe the validation related to the satellite HONO products developed in DINAR. This report includes details of all validation activities performed based on aircraft data as well as satellite-satellite comparisons. It should be noted that, because HONO is a new satellite development, no specific requirements on the HONO column product quality have been defined so far. This contrasts with many existing satellite trace gas products.

Validating the satellite HONO products poses challenges due to the limited availability of independent column data of pyrogenic HONO, primarily sourced from aircraft campaigns. These data exhibit notable differences in spatial and temporal representativeness compared to the relatively coarse pixel size of the satellites (TROPOMI: 3.5x5.5 km^2, IASI: 12 km diameter at nadir).

Theys et al. (2020) compared TROPOMI HONO slant columns (SCDs) with aircraft zenith-sky DOAS measurements (see examples in section 3), e.g., during the Rabbit Foot Fire in Idaho (August 12, 2018), part of the BB-FLUX field study. Despite nearly synchronized measurements and identical DOAS techniques, comparing TROPOMI and aircraft data was challenging due to different sampling geometries, revealing fine-scale variability in HONO that satellite sounders could not resolve. Moreover, the large impact of smoke aerosols on the satellite measurement sensitivity was found to be an important source of discrepancy between the satellite and aircraft HONO observations. Here, we revisit these comparisons for the HONO vertical columns (VCDs) using an explicit aerosol correction.

An additional difficulty for IASI is that the aircraft campaigns of biomass burning events are typically conducted during the daytime, relatively distant from IASI's early morning and early evening overpasses. While IASI detected HONO enhancements in the Rabbit Foot Fire plume, the observations were hundreds of kilometers downwind from the aircraft data and occurred at nighttime, several hours after the aircraft measurements. Therefore, a dedicated validation methodology for the IASI HONO product should be carefully designed in the future, contingent upon the availability of exploitable third-party datasets.

Despite the associated challenges and large uncertainties, the cross-comparison between satellite products offers an interesting alternative. This is the subject of Section 2. A large focus is on the comparison of IASI and TROPOMI, but other data sets are considered, namely from the Cross-track Infrared Sounder (CrIS) and the Geostationary Environment Monitoring Spectrometer (GEMS). In section 3, the evaluation of TROPOMI HONO VCDs against BB-FLUX aircraft measurements is presented. The satellite uncertainties and comparison challenges are discussed in Section 4.

Acknowledgements:

We thank Rainer Volkamer (University of Colorado, Boulder) and the BB-FLUX team for sharing the data from the BB-FLUX campaign (https://data.eol.ucar.edu/project/BB-FLUX) and for fruitful discussions on the satellite vs aircraft comparison.

We acknowledge Gaelle Dufour (Université de Paris and Univ Paris Est Creteil) for providing the HONO CrIS data and her participation in the interpretation of the TROPOMI vs CrIS comparison.

2 Satellite-satellite intercomparison

2.1 Comparison of TROPOMI and IASI

Figure 2.1 illustrates all the confirmed HONO detections achieved with the IASI (2007-2023) and TROPOMI (2018-2023) observations throughout their entire time series, on 1° x 1° grids. The grid cells are color-coded based on the month with the most HONO detections. IASI and TROPOMI distributions align in mid and high latitudes (typically, beyond 35° N and S), showing consistent peak detections in local summer (May-September in the Northern Hemisphere, November-February in the Southern Hemisphere). However, noteworthy differences emerge in tropical biomass burning regions, where IASI notably misses many TROPOMI detections. For example, IASI captures only limited pyrogenic HONO in southern Amazonia and southern Africa, and almost no HONO in West Africa and Southeast Asia, while TROPOMI exhibits more extensive detections during the dry season of these regions. Causes for such missed detections are discussed below.

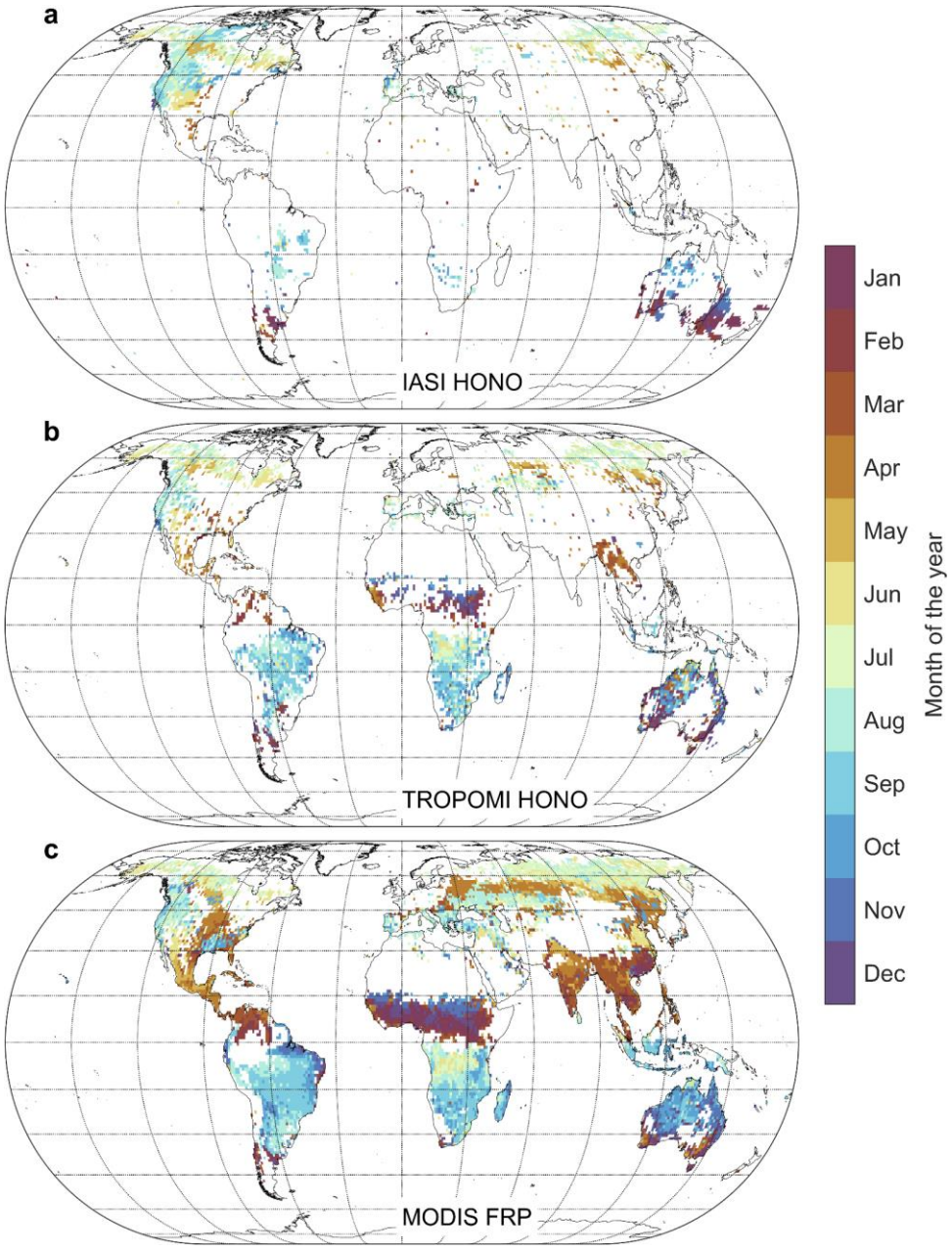

Figure 2.1. (a-b) Month of the year with the most HONO detections from IASI (2007-2023) and TROPOMI (2018-2023) on a 1° x 1° grid. (c) Month of the year with the highest cumulative MODIS/Terra fire radiative power (FRP) on the same grid. Filters on the number of MODIS active fires detections (>50 grid cell) and cumulative FRP (>200 MW per grid cell) allow excluding regions with less biomass burning activities. This figure is taken from Franco et al. (2023).

Figure 2.1 also displays the month with the highest cumulative fire radiative power (FRP) from MODIS, which serves as a satellite metric of fire intensity (e.g., Rogers et al., 2015; Giglio et al., 2016). The MODIS distribution shows that in areas where HONO is detected using TROPOMI and/or IASI, the peak HONO occurrences align with the period of most vigorous fire activity. This correlation supports observations from TROPOMI, indicating an increase in HONO abundance and of the HONO/NO2 ratio with rising FRP in wildfire plumes (Fredrickson et al., 2023), and highlights the strong link between HONO production and fire intensity.

As described by Franco et al. (2023), two factors contribute to IASI's less frequent detection of HONO in tropical biomass burning regions compared to TROPOMI:

- low HONO concentrations: MODIS data reveal that, although the Tropics experience more frequent wildfires, they are typically of smaller extent and of lower intensity than those in mid and high latitudes (Giglio et al., 2006; Luo et al., 2017; Andela et al., 2019; Haas et al., 2022). Since HONO production is closely linked to fire intensity, IASI is more likely to detect HONO in the more intense wildfires in mid and high latitudes (e.g., in North America and Siberia) than in tropical regions. Moreover, given IASI's coarser spatial resolution (12 km diameter at nadir compared to TROPOMI's 3.5×5.5 km^2), the same HONO quantity concentrated within a fire plume becomes more dispersed within an IASI pixel. Hence, detecting lower HONO concentrations becomes more challenging or even impossible compared to TROPOMI.
- weak thermal contrast (TC): IASI's sensitivity is mostly driven by TC (temperature difference between Earth's surface and an atmospheric layer), and hence by fire plume altitudes. In mid and high latitudes, where intense fires generate higher-altitude plumes, TC is typically larger and IASI's sensitivity is optimal, facilitating HONO detection. However, IASI has a limited sensitivity to lower atmospheric layers, where tropical fire plumes are prevalent, due to weaker TC. In contrast, TROPOMI, with more homogeneous sensitivity across altitudes, can detect HONO in a broader range of plume heights, including those typical of tropical fires. The typical vertical sensitivity of IASI and TROPOMI is discussed in section 4.

In order to provide a first quantitative assessment of the IASI and TROPOMI's HONO products, we have performed an inter-comparison between the HONO VCDs retrieved by the two sounders in the fire plumes of two case studies: the Woolsey Fire (California, November 8, 2018; Fig. 2.2) and Yakutian wildfires (Siberia, August 2, 2021; Fig. 2.3). For IASI, we used the VCDs from the ANNI v4 HONO product (Franco et al., 2023; described also in the ATBD), assuming here a constant altitude of the fire plumes at 5 km. For TROPOMI, the measured SCDs were converted to HONO VCDs assuming an air mass factor (AMF) of 0.3. This value was found to be appropriate for

the high aerosol optical depths (AOD) of the studied fires and for the fire plume height (5 km).

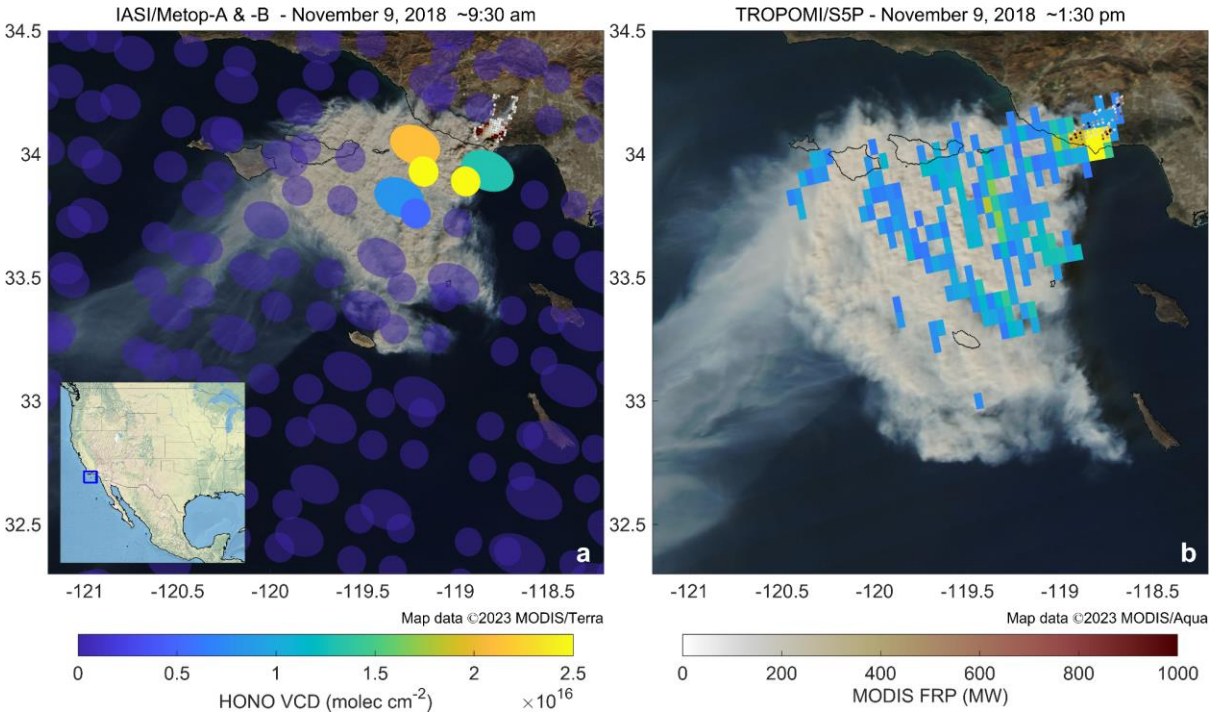

Figure 2.2. HONO VCDs from IASI (~9:30 AM) and TROPOMI (~1:30 PM) during the Woolsey Fire, California (November 9, 2018). The shape of each IASI dot corresponds to the footprint on the ground of a measurement. The dark blue IASI pixels indicate measurements without HONO detections. The small white/reddish dots indicate the FRP values of active fires detected by MODIS/Terra (~10:30 AM) and -Aqua (~1:30 PM), coincident with the IASI and TROPOMI measurements. This figure is taken from Franco et al. (2023).

Direct comparisons between IASI and TROPOMI VCDs in the same fire event are not trivial to interpret considering the intrinsic differences between the two sounders, such as: (i) the spatial resolution, with 12 km diameter at nadir for IASI vs. 3.5 x 5.5 km² for TROPOMI; (ii) the overpass time, with 9:30 AM/PM for IASI vs. 1:30 PM for TROPOMI; (iii) IASI's sensitivity influenced by the fire plume altitude (see section 4); (iv) the impact of smoke aerosols on TROPOMI's retrievals (see section 4). Despite these differences, we observe, in the two case studies, a concurrence in magnitude of retrieved HONO VCDs, with typical values falling within the range of 0.5 - 2.5 x 10^{16} molec/cm². Consistently, the highest VCDs are generally found in the vicinity of the fires (identified here by elevated MODIS FRP values), especially in daytime (see below), and rapidly decrease away from the sources due to the short atmospheric lifetime of HONO.

However, discrepancies between IASI and TROPOMI are noteworthy. As mentioned earlier, these differences can be attributed, firstly, to the higher spatial resolution and vertical sensitivity of TROPOMI. The two fire events studied here indeed emphasize TROPOMI's ability to detect HONO in closer proximity to the fire sources as well as in smaller fire plumes compared to IASI, whose HONO measurements are relatively limited to the most concentrated parts of the main fire plume. The difference in overpass times between the two satellite sounders explains another aspect of the observed discrepancies. The daytime IASI observations (9:30 AM) and the TROPOMI measurements (1:30 PM) of HONO occur relatively close to the fire sources. This is due to the intense photolysis during the daytime (the major atmospheric sink of HONO) that efficiently breaks down HONO molecules before they can be transported further downwind. Conversely, significant HONO enhancements are still captured at a long distance from the fire sources by the nighttime IASI measurements (9:30 PM). This is attributed to the absence of photolysis during the night, which significantly increases the lifetime of HONO, likely in combination with active secondary formation in the fire plumes.

Although other factors contribute to the uncertainties in the retrieved HONO VCDs from IASI and TROPOMI and to the observed discrepancies (see section 4), these case studies emphasize the convergence between the products of IASI and TROPOMI, as well as their complementarity in studying the abundance and diurnal variations of HONO in fire plumes.

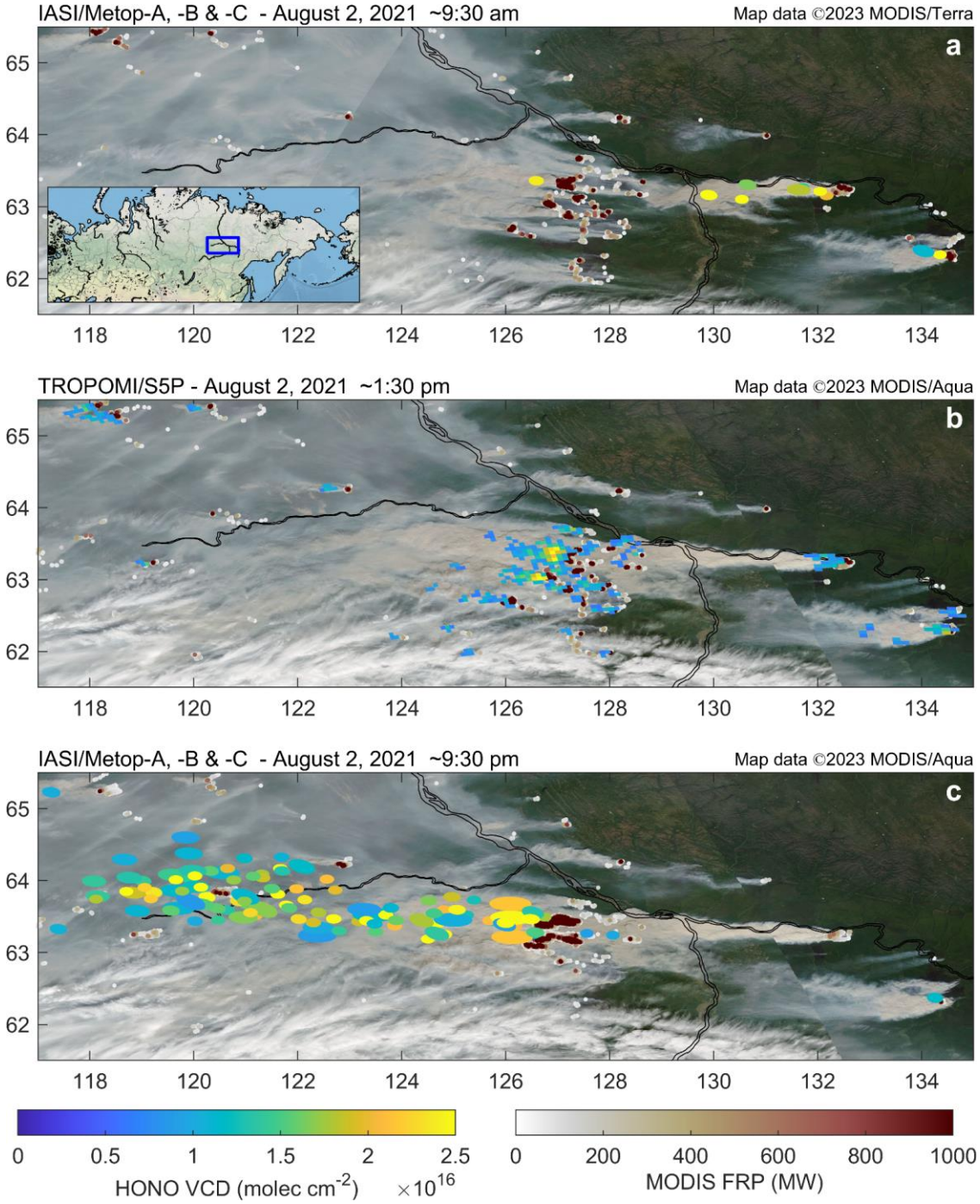

Figure 2.3. HONO VCDs from IASI (~9:30 AM/PM) and TROPOMI (~1:30 PM) during Yakutian wildfires (August 2, 2021). The shape of each IASI dot corresponds to the footprint on the ground of a measurement. The small white/reddish dots indicate the FRP values of active fires detected by MODIS/Terra (~10:30 AM/PM) and -Aqua (~1:30 PM), coincident with the IASI and TROPOMI measurements. This figure is taken from Franco et al. (2023).

Following the examples of TROPOMI-IASI comparison presented above, Figure 2.4 presents the global maps of HONO detections from IASI (separately for AM and PM observations) and TROPOMI, for the period from May 2018 to September 2023. Each data point corresponds to an observation for which HONO could be retrieved confidently, i.e., well above the detection limit (following the description in the DINAR ATBD). The displayed quantity is the HONO vertical column. For IASI, we used the HONO column based on the CALIPSO climatology of smoke plume altitude. For TROPOMI, the retrievals are heavily impacted by smoke aerosols. Given the wide range of aerosol conditions (in terms of AOD, optical properties, vertical distribution, etc.) expected at the global scale, a simplistic approach was considered. Similarly, as for the previous examples (Figures 2.2 and 2.3), a fixed air mass factor of 0.3 was consistently applied to convert the HONO SCDs into vertical columns. From radiative transfer simulations, this was found to be a reasonable value for high AODs and observed plume height conditions. This 'effective' AMF will obviously not be able to reproduce any detail of the radiative transfer and is mostly meant to benchmark the IASI retrievals.

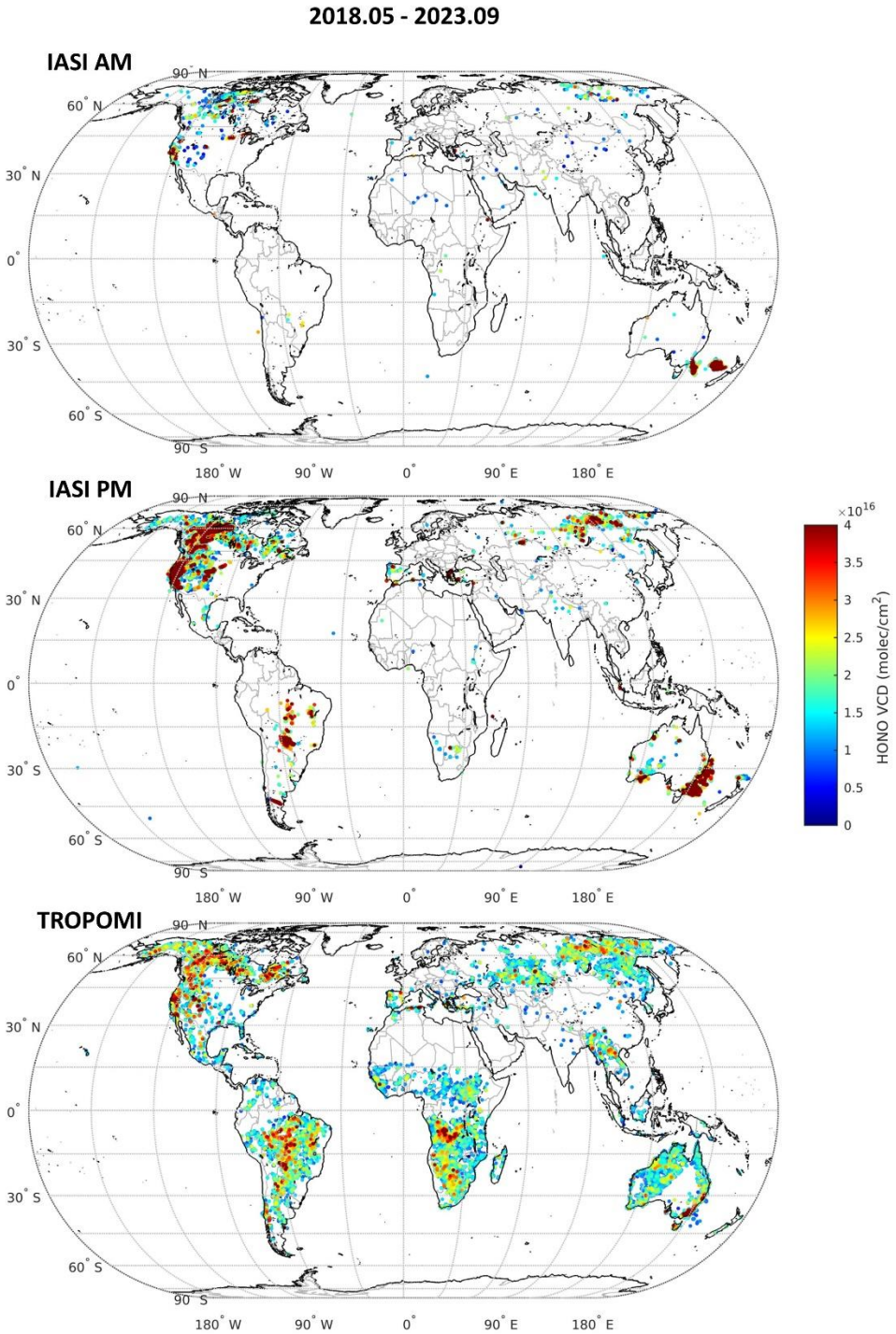

Figure 2.4. Global detections of HONO vertical columns for the period May 2018 to September 2023 from (top) morning and (center) evening observations of IASI, and (bottom) TROPOMI. The total number of detections are 2043, 14159, and 113746, by IASI AM, IASI PM and TROPOMI, respectively.

From Figure 2.4, one can see that the number of HONO detections by TROPOMI is much larger than with IASI. This is expected from the better measurement sensitivity in the UV to plumes in the lower troposphere. This is particularly visible in tropical biomass burning regions where HONO is barely detected by IASI. This feature is discussed above and is attributed to a combination of lower fire intensity and lower plume height in these regions. Apart from that, there are similarities between IASI and TROPOMI for mid- and high latitudes. E.g., HONO is detected in the same geographical regions, and the HONO vertical column values are of the same order of magnitude. Note also that there are more detections in the IASI evening observations than for the morning overpass (about 7 times more). This is due to the lower HONO photolysis during the night than for daytime (as discussed above and in Franco et al., 2023).

For a closer comparison, time series have been computed for both products for four different regions including Canada (50-70°N, 100-140°W), Western US (30-50°N, 110-130°W), Russia (55-70°N, 100-140°E) and Australia (25-45°S, 147-180°E). Figure 2.5 shows time series of HONO VCD for the selected regions.

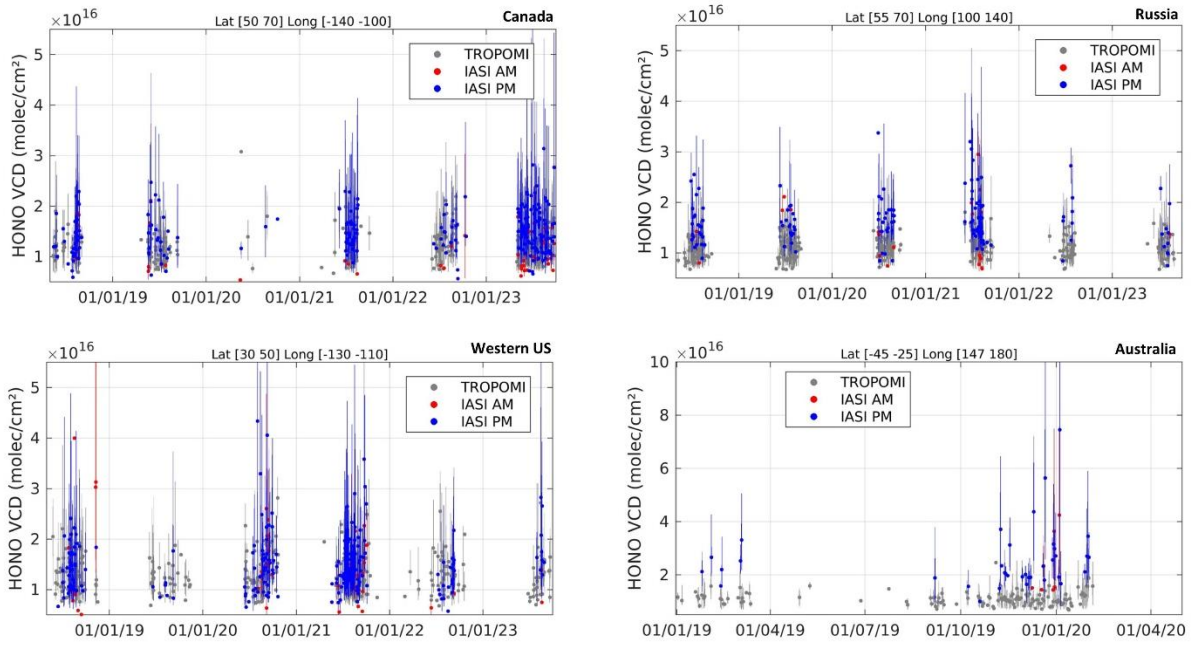

Figure 2.5. Time-series of daily averaged HONO vertical column from TROPOMI, IASI AM and IASI PM observations over Canada, Western US, Russia, and Australia. The latitude and longitude limits of the selected regions are indicated in the title of each plot. The error bars correspond to the 10 and 90 percentiles.

Overall, these results confirm that TROPOMI and IASI are rather similar with detections at the same period of the year and with VCDs of the same order of magnitude, albeit large data scatter. A direct comparison of TROPOMI and IASI is presented in Figure A.1 in Annex, in the form of scatter plots. In general, the TROPOMI and IASI data are poorly correlated. Consequently, a quantitative comparison between TROPOMI and IASI is difficult. As a complement of Figure 2.5, the mean and standard deviation of all HONO vertical columns from TROPOMI and IASI are shown in Figure 2.6, for the four selected regions.

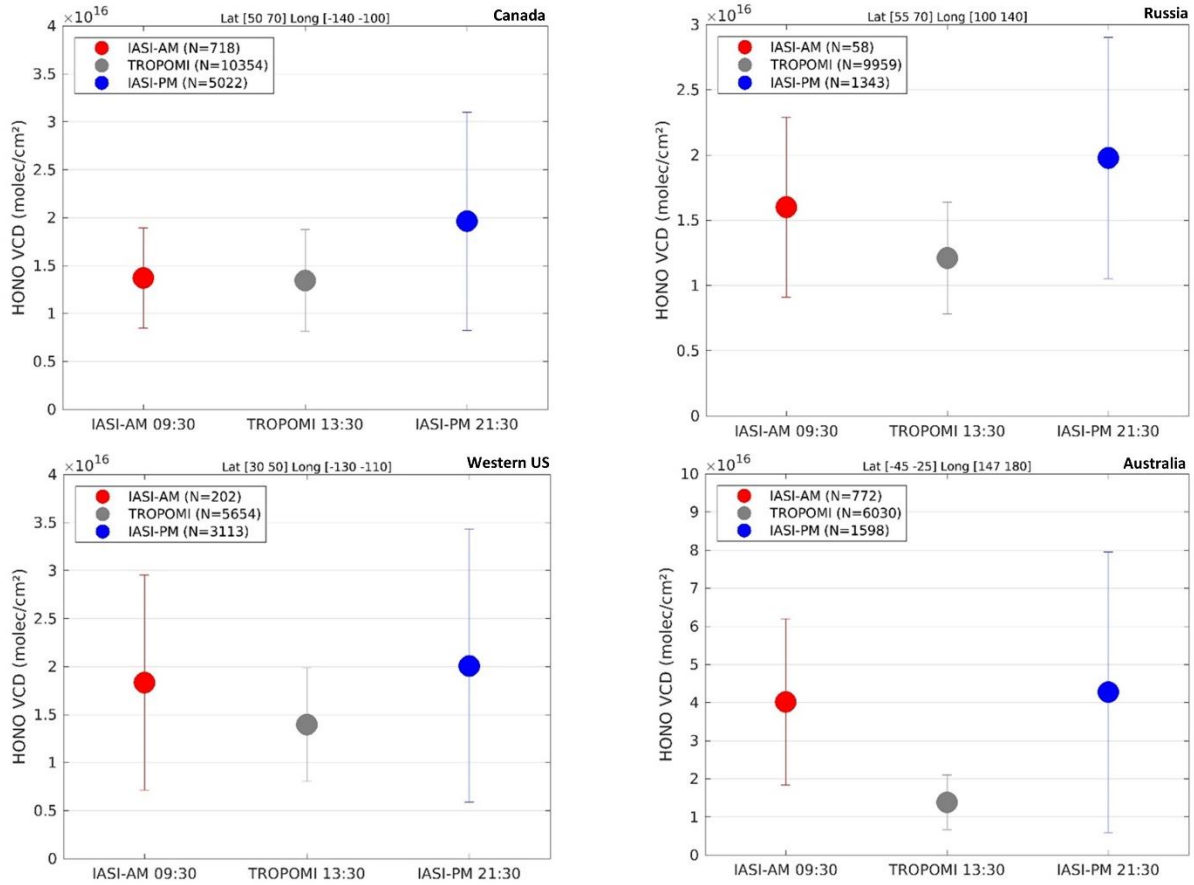

Figure 2.6. Mean HONO vertical column of all data from TROPOMI, IASI AM and IASI PM, for the selected regions shown in Figure 2.5. The error bars correspond to the standard deviation of the data. The number of pixels considered is indicated in the legend.

One can see that IASI PM results are generally higher than IASI AM data. Interestingly, the HONO VCDs during nighttime are also characterized by a larger scatter around the mean than during daytime. This is likely due to a combination of different elements: (1) many more detections during nighttime will lead to a large

chance of exceptionally high VCDs in the distribution, (2) weaker thermal contrast during nighttime, will lead to noisier retrievals, (3) lower HONO columns in the AM overpass (due to the shorter lifetime of HONO during the day) will imply that their scatter (in absolute value) is lower.

Overall, the agreement between IASI and TROPOMI in Figure 2.6 is satisfactory given the many sources of uncertainties and reasons for discrepancy. One exception is over Australia where the HONO VCDs from both IASI AM and PM are much larger than the TROPOMI results. The reason for this difference is not completely clear. We note however that results over Australia are mainly representative of the 2019/2020 fire season, which was exceptional in its intensity resulting in many fire-induced convective events. The amounts of emitted trace gases and aerosols were so huge that we cannot rule out biases in the retrievals (both in the UV and infrared) due to spectral interferences and complex radiative transfer in the plume.

2.2 Comparison of TROPOMI and CrIS

Dufour et al. (2022) reported on a fire plume from the Australian megafires during the 2019/2020 fire season, with elevated HONO levels that could be measured by the Cross-track Infrared Sounder (CrIS) aboard the Suomi National Polar-orbiting Partnership (S-NPP) platform. Here we compare the results from CrIS to those from TROPOMI for one day in particular (4th January 2020), over the Southeast part of Australia (Figure 2.7). The advantage of this comparison is that both instruments have nearly the same overpass times (a few minutes difference only). Compared to the initial results of Dufour et al. (2022), the CrIS retrievals shown on Figure 2.7 have been improved in two ways (G. Dufour, personal communication). First, a more realistic plume height of 11 km (instead of 4km) was used to invert the HONO vertical columns. Secondly, the convergence criterion has been fine-tuned (relaxed) to allow more valid pixels to be part of the comparison. Note that for TROPOMI the same assumption on the air mass factor (AMF=0.3) as before, was considered for the SCD to VCD conversion. To complement CrIS and TROPOMI, Figure 2.7 also shows the HONO VCDs obtained from IASI-B PM observations. IASI-B passed about 7h30 after CrIS and TROPOMI and witnessed the transport of the HONO plume over the Tasman sea, hundreds of kilometers South-East of the fire sources.

The images in Figure 2.7 show that HONO was detected over many fires, and the observed HONO plumes even extended further downwind. The measured HONO vertical columns were exceptionally high, up to 6 x 10^{16} molec/cm^2, the same order of magnitude being observed by TROPOMI, CrIS and IASI. However, the patterns observed by CrIS and TROPOMI are strikingly different. While TROPOMI mainly

detects enhanced HONO values near the fire sources, CrIS generally reports the highest HONO vertical columns much further away.

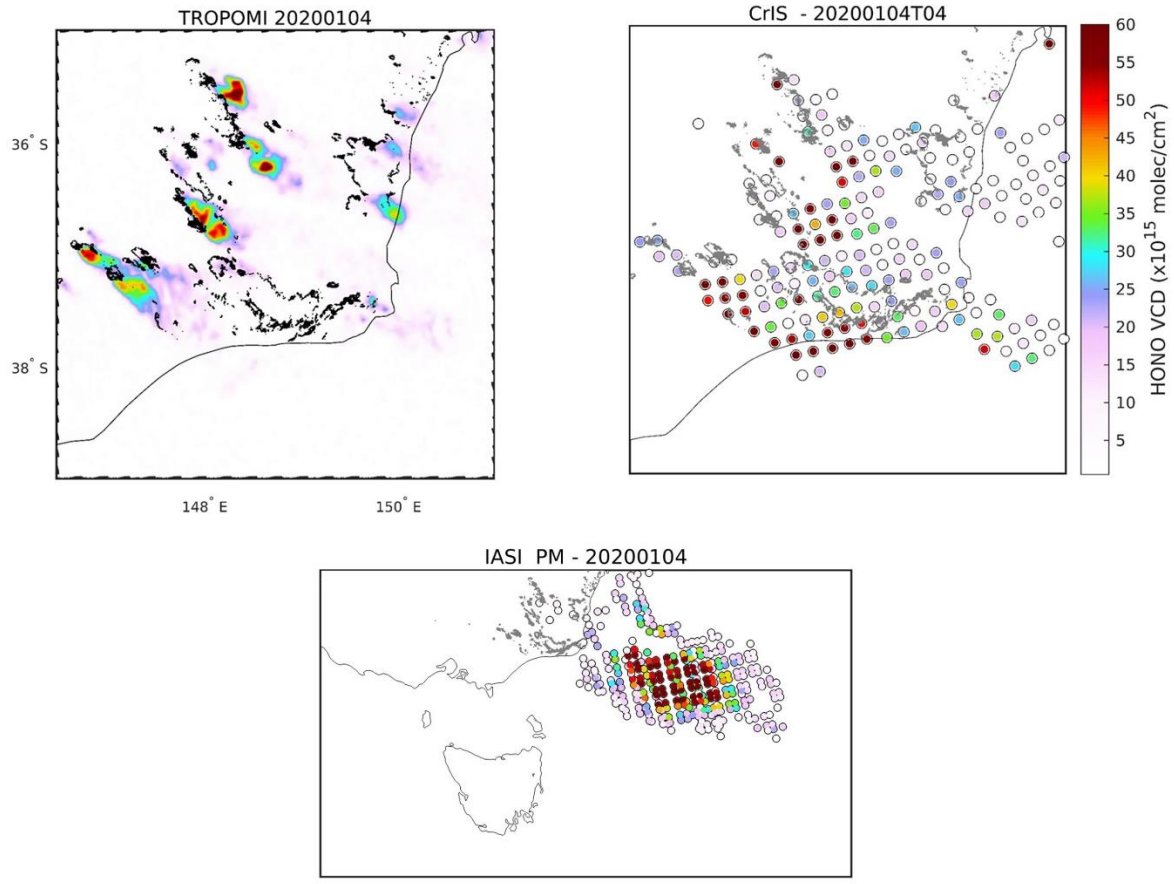

Figure 2.7. Comparison of HONO vertical columns from (top left) TROPOMI daytime, (top right) CrIS daytime and (bottom) IASI-B nighttime observations, for the 4th of January 2020, over Southeast Australia. The black dots indicate the fire locations as detected from VIIRS/S-NPP.

At the time of writing, the reason for the difference between TROPOMI and CrIS is not clear. However, by inspecting other cases, we found that the IASI HONO dataset tends to follow the same behavior as CrIS, i.e., HONO being detected at longer distance from the fires than with TROPOMI. This result may indicate that UV and IR soundings of optically dense smoke plumes are fundamentally different (and thus complementary). The reader is referred to section 4 for a discussion on comparison challenges. It should also be stressed that the CrIS retrievals are subject to several approximations (G. Dufour, personal communication), and currently it is difficult to conclude about this comparison, apart from the fact TROPOMI and CrIS HONO VCDs are of the same order of magnitude.

Unfortunately, this event is also the only available case for which TROPOMI and CrIS can be compared. In the future, it would be valuable to further compare TROPOMI and CrIS data, should a global CrIS HONO column product become available.

2.3 Comparison of TROPOMI and GEMS

As a demonstration of the retrieval of HONO from space, we adapted the DINAR TROPOMI algorithm and applied it to the spectra from the Geostationary Environment Monitoring Spectrometer (GEMS). For this exercise, we restricted the analysis to the HONO SCDs. A comparison of the results from GEMS and TROPOMI is given in Figure 2.8, for the data over Southeast Asia for March and April 2021-2023. Over that period of the year, agricultural and forest fires are known to occur in countries like Laos and Myanmar. These fires can have a significant impact on the pollution levels in the region and often beyond.

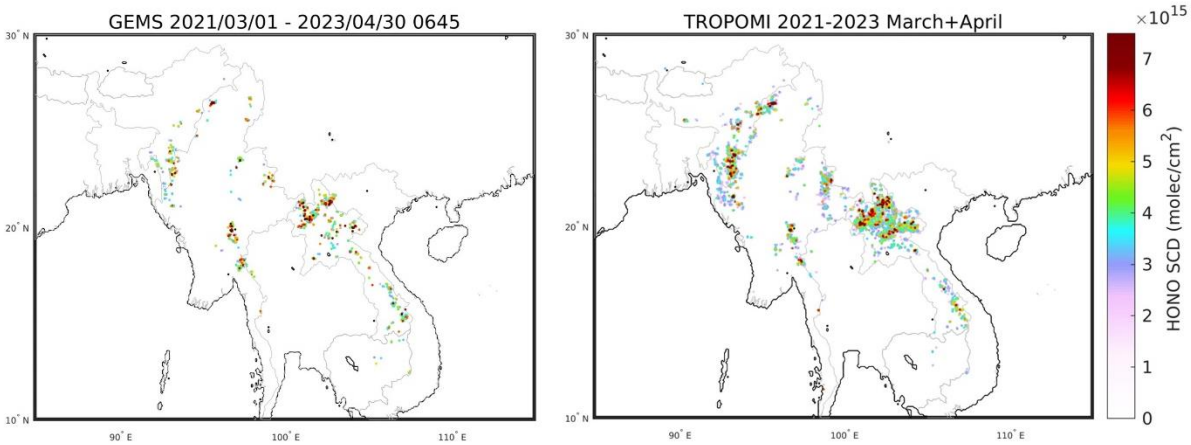

Figure 2.8. Comparison of HONO slant columns from (left) GEMS and (right) TROPOMI observations over Southeast Asia, for the months of March and April and for the years 2021-2023. For GEMS, only the results for the scan at 06h45 UTC are shown (close to the TROPOMI overpass time). GEMS and TROPOMI data are selected using the same selection criteria based on a detection flag. As described in the DINAR ATBD, the flag is based on the signal-to-noise ratio and informs on the confidence of the detection of HONO.

Overall, TROPOMI and GEMS results are in good agreement, at least qualitatively. Enhanced HONO is consistently detected in the same regions, notably in the northern part of Laos, in several locations in Myanmar near the border of India and further South close to Thailand. Quantitatively, the HONO SCDs agree well for the high values,

the maximum SCD being as high as 1.04 x 10^{16} molecules.cm^{-2} and 1.15 x 10^{16} molecules.cm^{-2}, for TROPOMI and GEMS respectively. However, the number of detections with TROPOMI (3485) are higher than with GEMS (934) and are typically found for lower HONO SCDs. This can be explained by the improved detection limit of TROPOMI compared to GEMS. The noise on the data being a factor of two lower, more pixels (with lower SCDs) will therefore pass the selection criteria.

It should be noted that the HONO retrievals are highly dependent on the time of observation and the spatial sampling. A proper comparison between TROPOMI and GEMS would need to account for this. Moreover, Figure 2.8 compares the HONO SCDs. More work is needed to calculate and compare HONO VCDs using consistent and realistic assumptions on the radiative transfer.

3 TROPOMI HONO VCD: Evaluation against aircraft measurements (BB-FLUX)

To test the accuracy of TROPOMI data, the HONO vertical columns are compared to aircraft measurements of wildfire plumes. As discussed in the DINAR Requirement Baseline Document, Section 4, there are only a handful of aircraft campaigns that could be used to evaluate HONO data from space. Here we use measurements acquired during the Biomass Burning Fluxes of Trace Gases and Aerosols (BB-FLUX) field study conducted in the US Pacific Northwest during the summer of 2018 wildfire season (Volkamer et al., 2020). The aircraft, equipped with a zenith-sky DOAS instrument, performed 37 research flights in total, over different wildfires during the period of the campaign. For each case, the aircraft flew under the smoke layer and performed several perpendicular traverses of the same plume. One particularity of the BB-FLUX HONO data is that the results were obtained using a remote sensing technique and with spectral retrieval settings very close to that of TROPOMI. Therefore, the HONO vertical columns can be compared more directly. This contrasts with most of the available HONO measurements in biomass burning plumes that are from in situ instruments (and that are representative only of a certain height). Another appealing aspect of the BB-FLUX campaign is that a small number of research flights were planned near the TROPOMI overpass time. This is particularly important for the validation, as fires plumes are highly heterogeneous environments, and the concentrations of HONO will vary strongly in space and time.

In the initial TROPOMI HONO paper (Theys et al., 2020), BB-FLUX data from three research flights (namely for the Rabbit Foot fire on 12 and 15 August 2018, and the Watson Creek fire on 19 August 2018) were exploited to validate the enhancement ratios of the HONO SCD to the NO_2 SCD (RHN), as measured by TROPOMI. Comparing RHNs was justified by the fact that it allows to cancel differences in air mass factors (AMF) that arise from different sampling geometries. Here we propose to revisit these three cases and go one step further by comparing estimations of HONO vertical columns (instead of RHN). This implies calculating air mass factors accounting explicitly for the presence of aerosols, both for aircraft and satellite geometries.

Before entering the details, it is enlightening to compare first the measured HONO SCDs for the three cases. The comparison plots are shown on Figs 3.1, 3.2, 3.3 (top panels), respectively. Here we use the same data selection and comparison methodology as outlined in the initial study. In brief, for each fire plume, the TROPOMI results are compared to the aircraft data for the two traverses closest in time to the satellite overpass (red and yellow dots on Figs 3.1-3.3). To improve the comparison, the data are aligned along a common plume age axis, to cope with (small) time differences between satellite and aircraft measurements. The reader is referred to the methods section of Theys et al. (2020) for further detail. As can be seen, TROPOMI generally underestimates largely the HONO SCDs observed by the aircraft, especially over the core of the plume. This can be understood as due to different retrieval sensitivity because of the different observation geometries, in particular for large AODs. Notably, the aircraft measurement integrated HONO over the entire wildfire plume, whereas the satellite measurement primarily sampled the top layer of the plume (see e.g., Figure S3 of Theys et al., 2020). It is interesting to note also that the aircraft data from the two traverses are generally consistent with each other, except for research flight 11 (Rabbit Foot fire, 12 August 2018) that exhibits large differences of HONO SCDs up to a factor of 4. However, for this case, the RHNs are in close agreement (see Fig 2c of Theys et al., 2020) suggesting a real HONO variability in the plume.

The next step is to calculate the AMFs for both geometries and compare the obtained VCDs (in the same way as the SCDs). For the aircraft, the measurement sensitivity is weakly dependent on the presence of aerosols and on plume height. Therefore, for all aircraft data, we used a fixed AMF of 1.5, a typical value obtained from radiative transfer simulations in the zenith-sky geometry (Figure S3 of Theys et al., 2020). For TROPOMI, the situation is different, and the calculation requires input values for the plume height, AOD and single scattering albedo (SSA). As the DINAR HONO algorithm tabulates vertical column values (for each pixel) as a function of these three

parameters, the HONO VCD is obtained simply by interpolation. Note that if an uncertainty on one parameter exists and can be estimated, it is easy to calculate the resulting error on the VCD. Individual error terms can then be added in quadrature to form the total VCD error. For the plume height, we used values between 3 and 4 km a.g.l., depending on the case. These were estimated by analyzing TROPOMI aerosol layer height product and CALIOP data. For the AOD and SSA, we first investigated the results from the TROPOMI UV aerosol product (TROPOMAER (at 354 nm); Torres et al., 2021), as a potential information source. Figure A.2 (left panels) in Annex shows examples of AOD maps for the three case studies. As shown, it appears that the aerosol product has data gaps, notably in the core of the fire plumes (i.e., for many of the pixels where HONO is detected). This is seen for cases 1 (top) and 3 (bottom). For case 2 (center), the aerosols map shows no gap, and the TROPOMAER AOD and SSA results have been used directly as input of the TROPOMI AMF calculation. For cases 1 and 3, we have used calculated AODs at 355 nm from observations made during BB-FLUX using the Solar Occultation Flux instrument (Volkamer et al., 2023). Results are displayed on Figure A.2, overlayed on the satellite AOD map (left panels), and plotted as a function of observation time, together with the coincidently measured HONO SCD data (right panels). Overall, the AOD is quite variable ranging between 5 to 20 for the core of the plumes. Based on this, we have considered for the TROPOMI AMF calculation, fixed (plume averaged) AODs of 7.5 and 10, for cases 1 and 3 respectively. For the SSA, we assumed an intermediate and fixed value of 85%.

The comparison results of HONO VCDs are shown on Figs 3.1, 3.2, 3.3 (bottom panels), for the three cases respectively. The error bars on the TROPOMI column estimates correspond to the error propagation of uncertainties on the AMF input parameters, as detailed in the figure captions. Overall, the TROPOMI VCDs agree reasonably well with the aircraft estimates. The low bias of TROPOMI with respect to the aircraft data seen in the SCD comparison is basically solved with the VCD calculation. This gives some confidence in the TROPOMI HONO retrievals. However, it is clear that the uncertainties remain very large. Similarly, the HONO variability and sampling differences between the satellite and aircraft are significant.

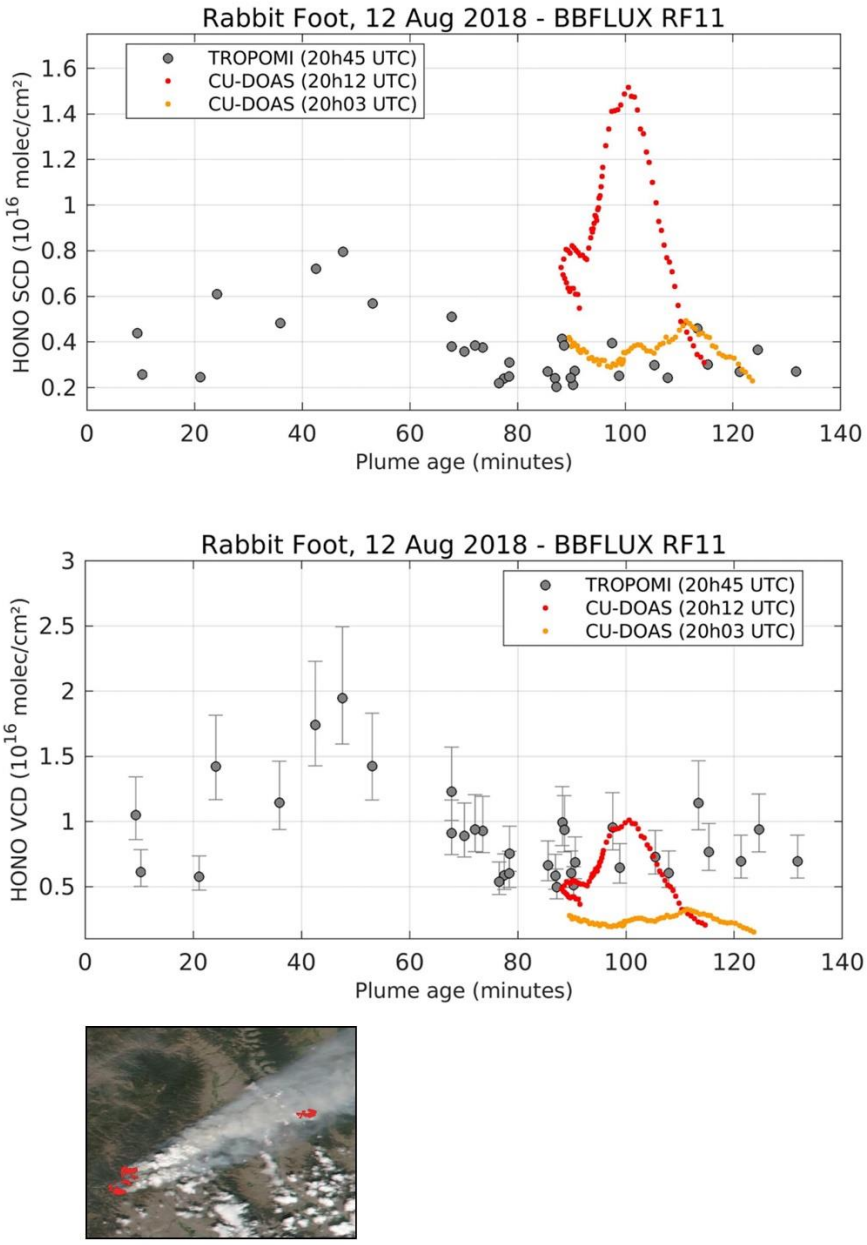

Figure 3.1: (top) Comparison of HONO SCDs from TROPOMI (gray) and aircraft CU DOAS instrument (red and yellow dots, for two perpendicular traverses of the plume), for the Rabbit Foot fire on 12 August 2018. The results are plotted as a function of plume age. Note that the TROPOMI data for plume age less than 80 minutes correspond to the pixels near the fire sources and are not sampled by the aircraft, that typically flew >50km downwind of the fires. (bottom) Same for HONO VCDs. For TROPOMI, the AMFs are calculated for AOD of 7.5±1, SSA of 85 ±2.5 % and plume height of 3±1 km. The inset image is a composite of true-color RGB image with fire

detection and thermal anomaly product (red points) from the VIIRS/Suomi-NPP instrument (https://worldview.earthdata.nasa.gov/), which shows smoke aerosols and the fire source locations.

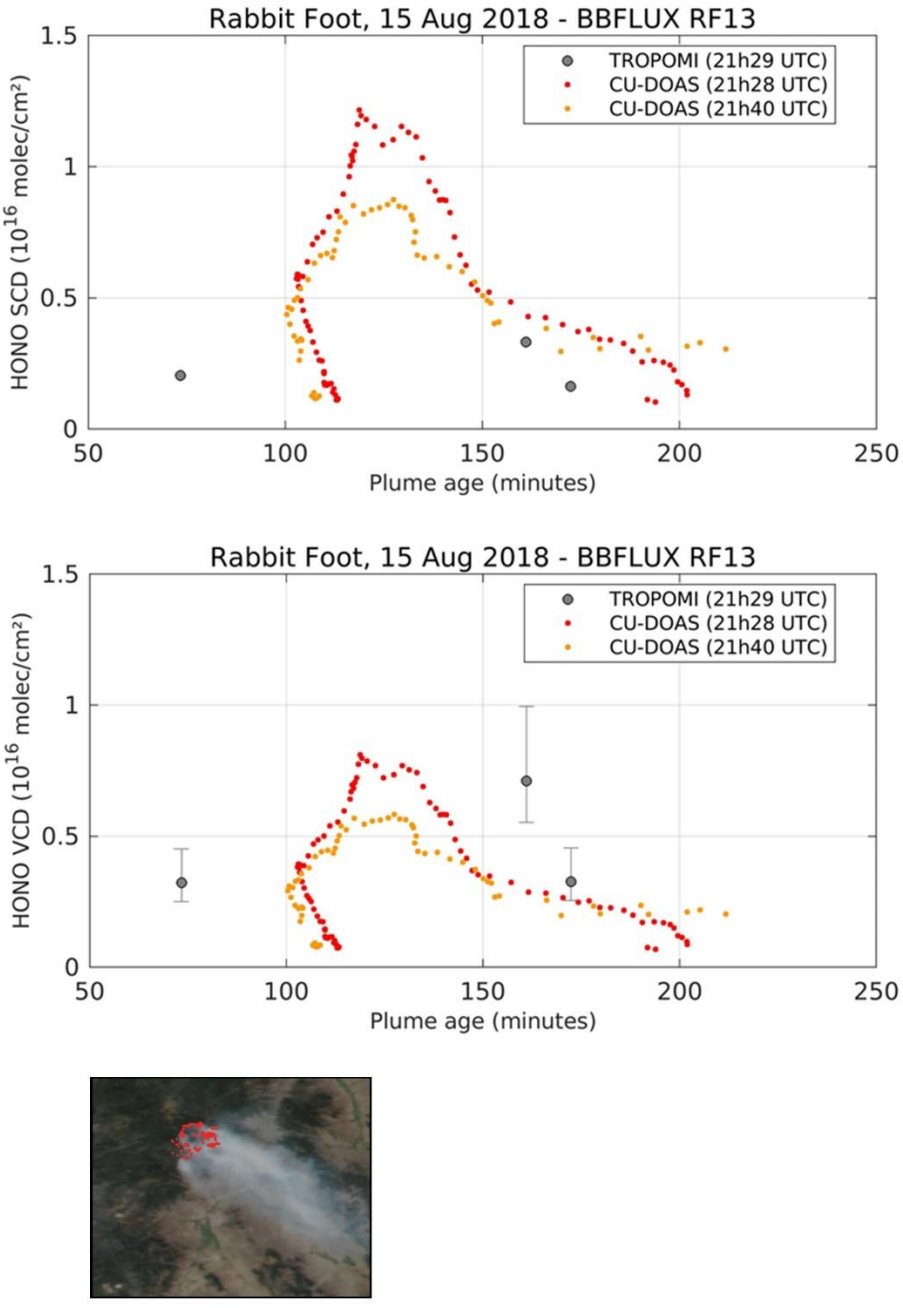

Figure 3.2: same as figure 3.1 for the Rabbit Foot fire on 15 August 2018. For TROPOMI, the AMFs are calculated using input from the TROPOMAER product, for

the AOD (assumed uncertainty: ±1) and the SSA (assumed uncertainty: ±2.5 %). The plume height considered is of 3.5±1 km.

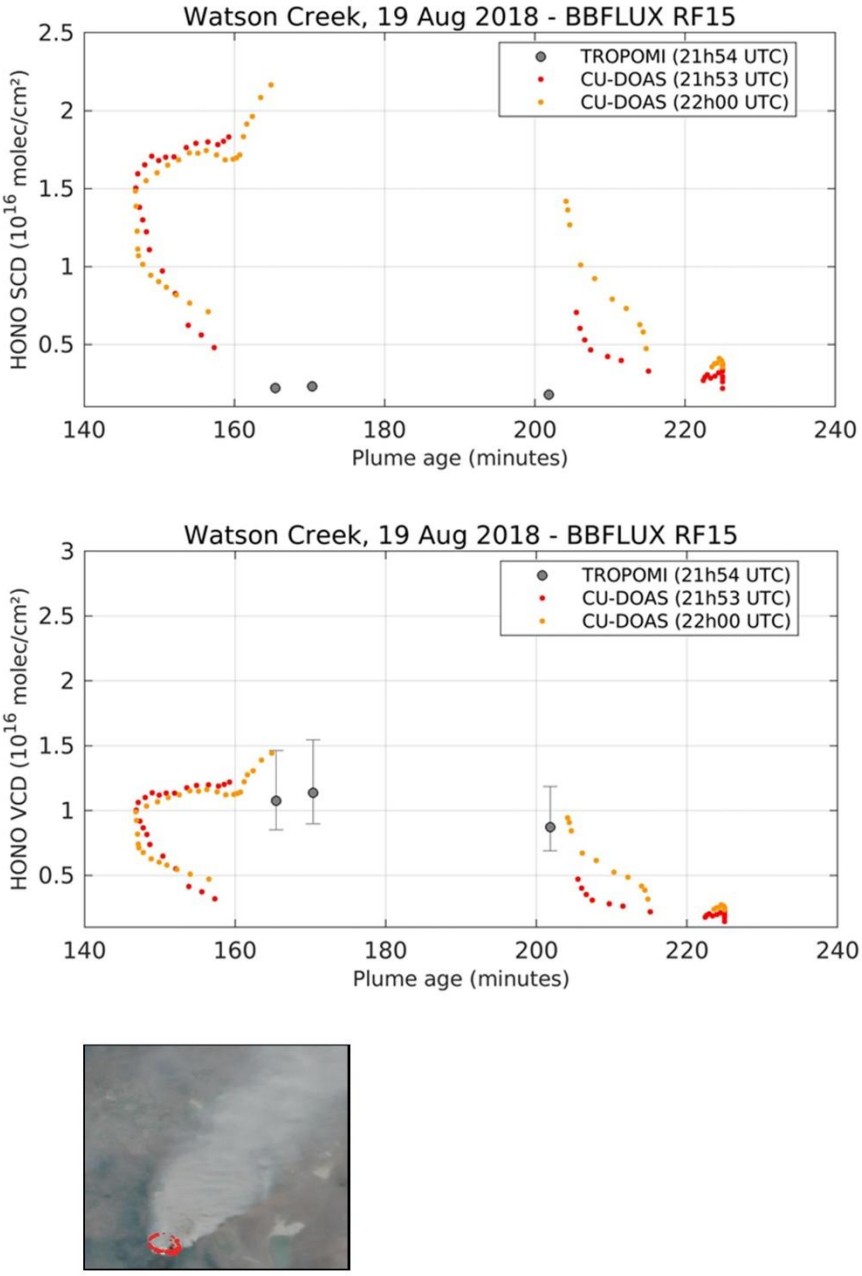

Figure 3.3: same as figure 3.1 for the Watson Creek fire on 19 August 2018. For TROPOMI, the AMFs are calculated for AOD of 10±1, SSA of 85 ±2.5 % and plume height of 4±1 km.

4 Discussion on satellite uncertainty and comparison challenges

Retrieving accurate HONO VCDs in fire plumes from both IASI and TROPOMI remains challenging. Current retrieval methods rely indeed on assumptions that introduce uncertainties on the retrieved VCDs, which in turn hinders a more precise comparison between their respective HONO products.

Based on Rogers (2000) and Bauduin et al. (2017), uncertainties (σ) on retrieved VCDs of a target species can be estimated from the generalized noise of the satellite sounder. Based on the US 1976 standard atmosphere and a surface temperature of 300 K, we have calculated these uncertainties on the retrieved HONO VCDs from IASI and TROPOMI, assuming that HONO is contained in narrow fire plumes located at various altitudes. For TROPOMI, the simulations assumed a SSA of 80% (fresh plume, absorbing aerosols) and an AOD of 5. From these uncertainties, a relatively conservative detection threshold of HONO can be obtained as 4σ. Results, reported in Fig. 4.1, show that IASI's detection threshold of HONO is high for low-altitude fire plumes (1.5-2.0 x 10^{16} molec/cm² for plumes within 1-2 km altitude), reflecting IASI's limited sensitivity to the lowermost atmospheric layers. However, this threshold decreases significantly at higher layers (<0.5 x 10^{16} molec/cm² for plumes above 8 km altitude) due to larger thermal contrast, indicating IASI's enhanced sensitivity to elevated fire plumes. Conversely, TROPOMI's detection threshold, in the range of 0.2-0.4 x 10^{16} molec/cm², is more homogeneous throughout the troposphere and significantly lower than IASI. This comparison emphasizes TROPOMI's ability to detect lower HONO concentrations and smaller fire plumes compared to IASI, especially with low-altitude fire plumes.

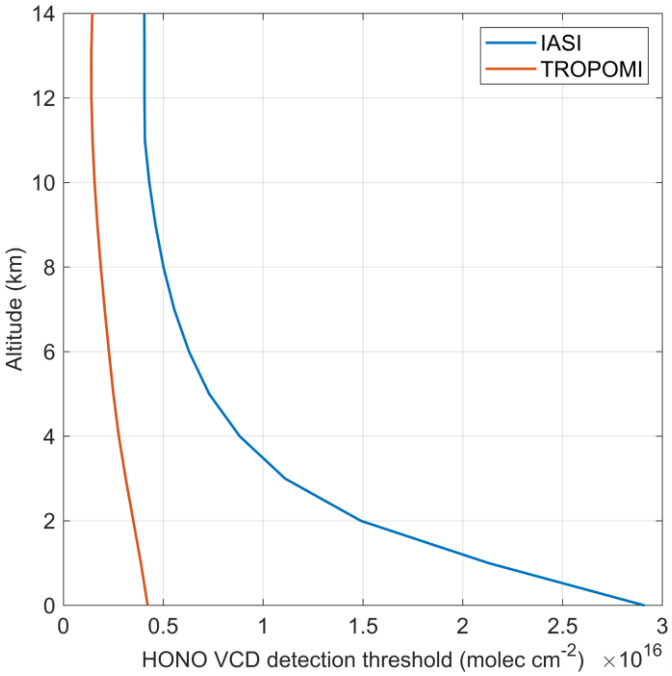

Figure 4.1. Typical IASI and TROPOMI's detection threshold of HONO vertical column densities (VCDs) according to the altitude of the fire plume containing HONO. This figure is taken from Franco et al. (2023).

The detection thresholds (and uncertainties) presented in Fig. 4.1 illustrate well that IASI-retrieved HONO VCDs are influenced by altitude and that their accuracy depends on the IASI's uneven vertical sensitivity. This can lead to biased retrieved VCDs if the altitude of the HONO peak assumed during the retrieval process differs significantly from the actual altitude of the fire plume where most HONO is present. While IASI's retrieval algorithm can accommodate various heights and thicknesses of the HONO layer, accurate information about the fire plume altitude is often challenging to obtain, especially for non-major fire events. Moreover, smoke plumes with rapidly changing altitudes present even more difficulties.

While TROPOMI's sensitivity is less dependent on the HONO vertical distribution compared to IASI, it is influenced by the presence of high concentrations of smoke aerosols. These absorbing aerosols rapidly enhance light extinction, limiting TROPOMI's ability to probe through the entire height of the smoke plume (Bousserez, 2014; Theys et al., 2020; Rowe et al., 2022). Consequently, determining the AMF necessary to convert the measured SCDs into HONO VCDs becomes challenging, introducing substantial uncertainties to the retrieved HONO abundance.

In presence of high aerosol loadings, TROPOMI primarily samples the upper layers of a smoke plume, where HONO undergoes rapid removal due to intense photolysis, but has limited or no sensitivity to HONO in the lower plume layers. This may account for

the shorter distance of HONO detections with TROPOMI from fire sources and the generally lower TROPOMI VCDs compared to IASI. IASI, which in contrast encounters less interference from smoke aerosols, potentially allows for the full-height probing of HONO inside the plume (Clarisse et al., 2010, 2013). As HONO might experience an increased lifetime inside the plume due to the limited light penetration and reduced photolysis, it contributes to explaining why IASI detects HONO even after substantial transport from fire sources, even during daytime.

Given the considerations above, establish a proper error budget of the TROPOMI and IASI HONO retrievals is very difficult, as it depends on the observation conditions and information on aerosols and plume height. Yet, we have calculated typical error estimates representative of TROPOMI and IASI HONO vertical columns. The results are summarized in Tables 1 and 2 below, separately for the random and systematic errors. As the information on plume height is important and allows to reduce the VCD error (as discussed above), two error estimates are calculated, including ("all") or not including ("lim") the plume height related uncertainty.

For TROPOMI, a typical HONO VCD of 1.5 x 10^{16} molecules/cm² is considered. For the AMF calculation, we assumed a plume height of 5 km, AOD of 5 and SSA of 80%. For the random uncertainty, only the error related to the spectral fitting part is considered; the estimated VCD random error is ~ 1.0 x 10^{15} molecules/cm². The systematic uncertainty on the HONO VCD is derived by propagation of errors from the spectral fit and AMF calculation steps. The systematic error from the fit is typically 10%. The AMF error has contributions from the different AMF input parameters. Here we use uncertainties on plume height of ±1km, AOD of ±2 and SSA of ±5% (note that the aerosols-related uncertainties taken here are higher /less optimistic than those used in Section3). The random and systematic errors on the HONO vertical column are summarized in Table 1. The error budget is dominated by systematic errors, mainly due to the uncertainties on the aerosol parameters.

For IASI, the Woolsey fire and Siberian fires (Figs 2.2 and 2.3) were considered. Random and systematic uncertainties were calculated for all observations (164 in total; mean column = 1.66 x 10^{16} molecules/cm²; std = 6.97 x 10^{15} molecules/cm²), following the error calculation of Clarisse et al. (2023) and using the settings outlined in the DINAR ATBD. The range of error values is provided in Table 2. Compared to TROPOMI, the random errors are larger. However, the systematic errors are clearly lower, and result from the fact that smoke aerosols have little influence on the infrared

sensitivity. This highlights again the complementarity between UV and infrared HONO retrievals.

Table 1. TROPOMI HONO vertical column error estimates.

Error type	**VCD error**
Random*	1.0 x 10^{15} molecules/cm^2
Systematic (all)	9.5 x 10^{15} molecules/cm^2
Systematic (lim)	9.1 x 10^{15} molecules/cm^2

* Error from the fit only.

Table 2. IASI HONO vertical column error estimates.

Error type	**VCD error range, mean (min-max)**
Random (all)	4.6 (2.6-9.0) x 10^{15} molecules/cm^2
Random (lim)	3.0 (2.0-4.0) x 10^{15} molecules/cm^2
Systematic (all)	2.6 (1.2-6.0) x 10^{15} molecules/cm^2
Systematic (lim)	1.9 (0.9-4.7) x 10^{15} molecules/cm^2

5 References

Andela, N., Morton, D. C., Giglio, L., Paugam, R., Chen, Y., Hantson, S., van der Werf, G. R., and Randerson, J. T.: The Global Fire Atlas of individual fire size, duration, speed and direction, Earth System Science Data, 11, 529–552, https://doi.org/10.5194/essd-11-529-2019, 2019.

Bousserez, N.: Space-based retrieval of NO2 over biomass burning regions: quantifying and reducing uncertainties, Atmospheric Measurement Techniques, 7, 3431–3444, https://doi.org/10.5194/amt-7-3431-2014, 2014.

Clarisse, L., Hurtmans, D., Prata, A. J., Karagulian, F., Clerbaux, C., De Mazière, M., and Coheur, P.-F.: Retrieving radius, concentration, optical depth, and mass of different types of aerosols from high-resolution infrared nadir spectra, Applied Optics, 49, 3713, https://doi.org/10.1364/ao.49.003713, 2010.

Clarisse, L., Coheur, P.-F., Prata, F., Hadji-Lazaro, J., Hurtmans, D., and Clerbaux, C.: A unified approach to infrared aerosol remote sensing and type specification, Atmospheric Chemistry and Physics, 13, 2195–2221, https://doi.org/10.5194/acp-13-2195-2013, 2013.

Clarisse, L., Franco, B., Van Damme, M., Di Gioacchino, T., Hadji-Lazaro, J., Whitburn, S., Noppen, L., Hurtmans, D., Clerbaux, C., and Coheur, P.: The IASI NH_3 version 4 product: averaging kernels and improved consistency, Atmos. Meas. Tech., 16, 5009–5028, https://doi.org/10.5194/amt-16-5009-2023, 2023.

DINAR project, Requirement Baseline Document (RBD), DINAR_HONO_RB_v3.0.pdf, 2022.

DINAR project, Algorithm Theoretical Baseline Document (ATBD), DINAR_HONO_ATBD_v2.0.pdf, 2024.

Dufour, G.; Eremenko, M.; Siour, G.; Sellitto, P.; Cuesta, J.; Perrin, A.; Beekmann, M. 24 h Evolution of an Exceptional HONO Plume Emitted by the Record- Breaking 2019/2020 Australian Wildfire Tracked from Space. Atmosphere 2022, 13, 1485. https://doi.org/10.3390/ atmos13091485.

Franco, B., Clarisse, L., Theys, N., Hadji-Lazaro, J., Clerbaux, C., and Coheur, P.: Pyrogenic HONO seen from space: insights from global IASI observations, EGUsphere [preprint], https://doi.org/10.5194/egusphere-2023-2707, 2023.

Fredrickson, C. D., Theys, N., and Thornton, J. A.: Satellite Evidence of HONO/NO2 Increase With Fire Radiative Power, Geophysical Research Letters, 50, e2023GL103 836, https://doi.org/10.1029/2023gl103836, 2023.

Giglio, L., van derWerf, G. R., Randerson, J. T., Collatz, G. J., and Kasibhatla, P.: Global estimation of burned area using MODIS active fire observations, Atmospheric Chemistry and Physics, 6, 957–974, https://doi.org/10.5194/acp-6-957-2006, 2006.

Giglio, L., Schroeder, W., and Justice, C. O.: The collection 6 MODIS active fire detection algorithm and fire products, Remote Sensing of Environment, 178, 31–41, https://doi.org/10.1016/j.rse.2016.02.054, 2016.

Haas, O., Prentice, I. C., and Harrison, S. P.: Global environmental controls on wildfire burnt area, size, and intensity, Environmental Research Letters, 17, 065 004, https://doi.org/10.1088/1748-9326/ac6a69, 2022.

Luo, R., Hui, D., Miao, N., Liang, C., and Wells, N.: Global relationship of fire occurrence and fire intensity: A test of intermediate fire occurrence-intensity hypothesis, Journal of Geophysical Research: Biogeosciences, 122, 1123–1136, https://doi.org/10.1002/2016jg003722, 2017.

Rogers, B. M., Soja, A. J., Goulden, M. L., and Randerson, J. T.: Influence of tree species on continental differences in boreal fires and climate feedbacks, Nature Geoscience, 8, 228–234, https://doi.org/10.1038/ngeo2352, 2015.

Rowe, J. P., Zarzana, K. J., Kille, N., Borsdorff, T., Goudar, M., Lee, C. F., Koenig, T. K., Romero-Alvarez, J., Campos, T., Knote, C., Theys, N., Landgraf, J., and Volkamer, R.: Carbon Monoxide in Optically Thick Wildfire Smoke: Evaluating TROPOMI Using CU Airborne SOF Column Observations, ACS Earth and Space Chemistry, 6, 1799–1812, https://doi.org/10.1021/acsearthspacechem.2c00048, 2022.

Theys, N., R. Volkamer, J.-F. Müller, K. J. Zarzana, N. Kille, L. Clarisse, I. De Smedt, C. Lerot, H. Finkenzeller, F. Hendrick, T. K. Koenig, C. F. Lee, C. Knote, H. Yu, and M. Van Roozendael: Global nitrous acid emissions and levels of regional oxidants enhanced by wildfires, *Nat. Geosci.*, ***13***, 681-686 (2020). https://doi.org/10.1038/s41561-020-0637-7.

Torres, O., et al. (2021), TROPOMI/Sentinel-5P Near UV Aerosol Optical Depth and Single Scattering Albedo L2 1-Orbit Snapshot 7.5 km x 3 km, NASA Goddard Space Flight Center, Goddard Earth Sciences Data and Information Services Center (GES DISC), Accessed: May 2023, 10.5067/MEASURES/AER/DATA204

Volkamer, R.; Kille, N.; Lee, C. F.; Zarzana, K. J.; Koenig, T.; Nutter, R.; Howard, B. J.; Knote, C.; Campos, T. L.; Oolman, L. D.; Plummer, D. M.; Deng, M.; Wang, Z.; Ahmadov, R.; Pierce, B.; Obersteiner, F.; Zahn, A.; Goulden, T.; Hass, B.; Hudak, A.; Restaino, J.; Ottmar, R. D. In The BB-FLUX Project: How Much Fuel Goes Up in Smoke? American Meteorological Society 100th Annual Meeting, 2020.

Volkamer, R. 2023. BB-FLUX: Calculated AirSOF AOD Data. Version 1.0. UCAR/NCAR - Earth Observing Laboratory. https://doi.org/10.26023/13AX-SFWT-290V . Accessed 12 Jan 2024.

6 Annex

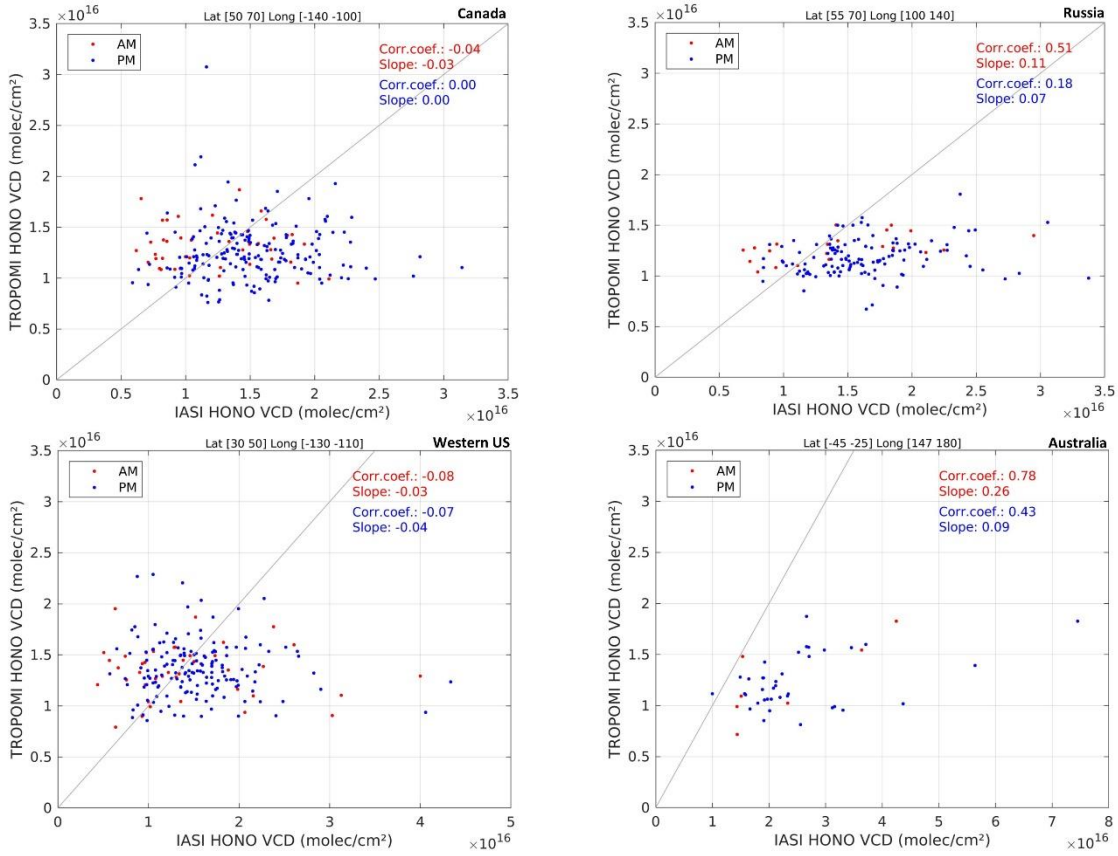

Figure A.1: Scatter plots of daily averaged HONO vertical column from TROPOMI, compared to IASI AM (red) and IASI PM (blue) observations over Canada, Western US, Russia, and Australia (as Figure 2.5). The correlation coefficient and slope of the regression line are given as an inset for each plot.

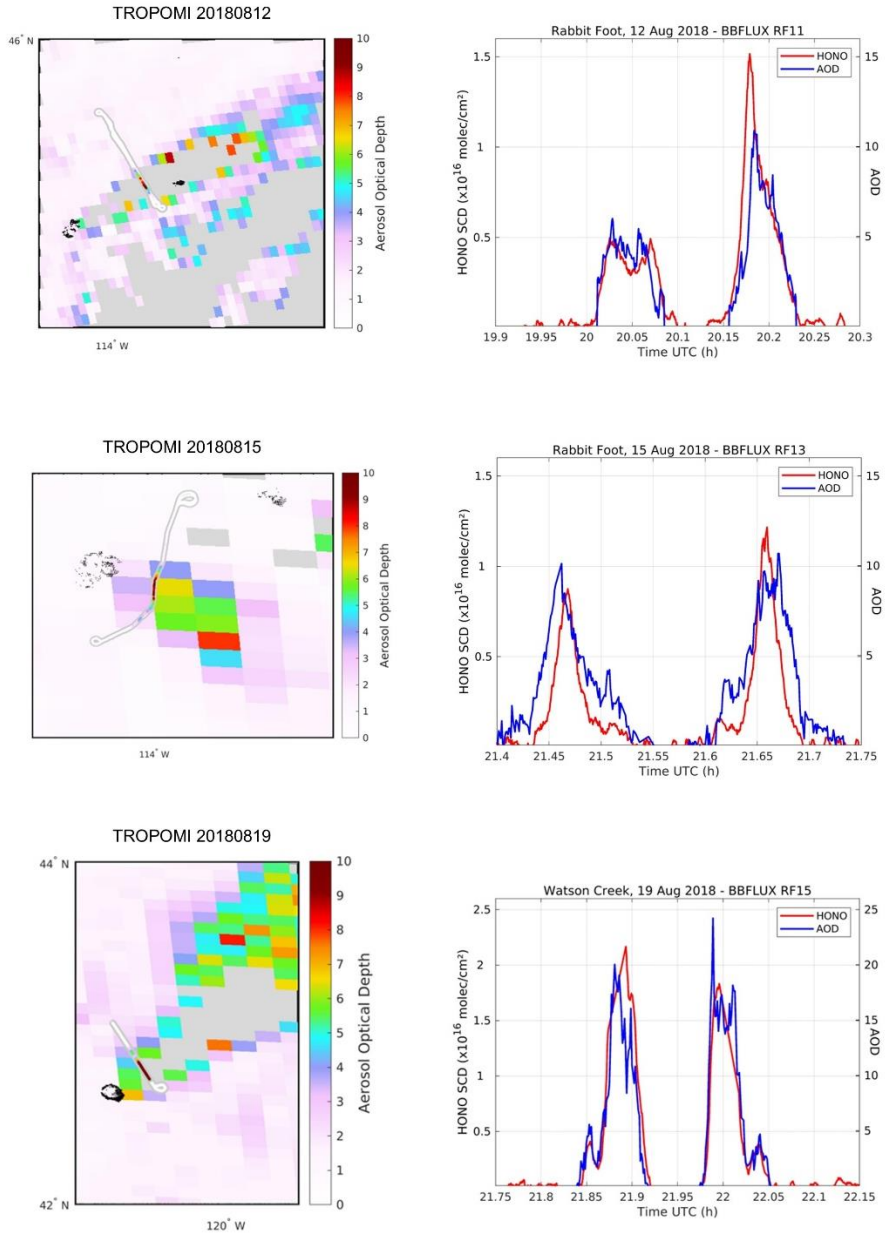

Figure A.2: (left) Aerosol optical depths from TROPOMI (Torres et al., 2021) and nearly synchronized aircraft measurements, for the Rabbit Foot fire on 12 August 2018 (top), 15 August 2018 (center) and Watson Creek fire on 19 August 2018 (bottom). The fires source locations are indicated by the black points (source: https://firms.modaps.eosdis. nasa.gov/). (right) Aircraft measurement of AOD (blue) and HONO SCD (red) as a function of observation time, for the three cases (from top to bottom).